Increase of magnetic and magnetoelectric properties in Co/Mn co-doped BiFeO3 multiferroic

Arij Marzouki, Vincent Loyau, Pascale Gemeiner, Lotfi Bessais, Brahim Dkhil, Adel Megriche

Increase of magnetic and magnetoelectric properties in Co/Mn co-doped $BiFeO_3$ multiferroic

Arij Marzouki[a,b,c]*, Vincent Loyau[d], Pascale Gemeiner[b], Lotfi Bessais[e], Brahim Dkhil[b], Adel Megriche[c]

a. Université Paris 13, Sorbonne Paris Cité, Laboratoire de Sciences des Procédés et des Materiaux, CNRS UPR-3407, 93430 Villetaneuse, France.
b. Laboratoire Structures, Propriétés et Modélisation des Solides, CentraleSupélec, CNRS-UMR8580, Université Paris-Saclay, 91190 Gif-sur-Yvette, France.
c. Université de Tunis El Manar, Faculté des Sciences de Tunis, UR11ES18 Unité de Recherche de Chimie Minérale Appliquée, 2092 Tunis, Tunisia.
d. SATIE UMR 8029 CNRS, ENS Cachan, Université Paris-Saclay, 61, Avenue du Président Wilson, 94235 Cachan Cedex, France.
e. CMTR, ICMPE, UMR7182, CNRS, Paris Est University, 2-8 rue Henri Dunant, 94320 Thiais, France.

*corresponding author: arij.marzouki@centralesupelec.fr

Abstract

Co and Mn co-doped $BiFeO_3$ samples are successfully realized using a stirred hydrothermal route to form $BiFe_{0.9}Co_xMn_{0.1-x}O_3$ (for x=0.01, 0.03, 0.05, 0.07 and 0.09) system. Our data show that both the ferroelectric (T_C) and antiferromagnetic (T_N) transition temperatures increase especially T_N varies by up to 23°C when changing from $BiFe_{0.9}Co_{0.01}Mn_{0.09}O_3$ to $BiFe_{0.9}Co_{0.09}Mn_{0.01}O_3$. Such strong T_N enhancement is explained by Co ionic size which induces a chemical pressure by reducing the unit cell and consequently favor the exchange coupling between the magnetic moments carried by Fe/Co/Mn. Moreover, Co^{3+} (d^6 electronic configuration) by replacing Fe (d^5) increases the magnetization reaching a value of 3.394 emu/g for $BiFe_{0.9}Co_{0.09}Mn_{0.01}O_3$, by favoring double exchange interactions. The direct magnetoelectric (ME) measurements on those samples show a significant increase of the ME coefficient with a value of 8.720 mV/(Oe.cm) for $BiFe_{0.9}Co_{0.05}Mn_{0.05}O_3$ i.e. up to 6 times higher than that of pure $BiFeO_3$. For Mn-rich compositions, because of a parasitic $Bi_{25}FeO_{40}$ phase and high electric losses, no intrinsic ME coefficient could be measured.

1. Introduction

Multiferroic materials, which show both magnetic and ferroelectric properties are still attracting considerable attention due to the fascinating fundamental physics underlying their behavior and potential applications allowing to control the magnetic (ferroelectric) response using an electric (magnetic) field through magnetoelectric coupling **[1]**. Of particular interest is $BiFeO_3$ (BFO), which exhibits both ferroelectric and antiferromagnetic properties at room temperature. Indeed, its ferroelectric Curie temperature (T_C ~1103 K) and antiferromagnetic Néel temperature (T_N ~643 K) are far above room temperature and make BFO a promising and attractive material for applications purpose. Bulk BFO crystallizes in a rhombohedral distorted perovskite structure *(R3c* space group), with anti-phase octahedral tilting and ionic displacements from the centrosymmetric positions about and along, respectively, a same <111> cubic-like direction. In addition to the G-type antiferromagnetic order, a cycloid-type spatial spin modulation (64 nm long) superimposes and is known to inhibit the linear magnetoelectric (ME) coupling in bulk BFO **[2]** leading to only a weak intrinsic ME coefficient with a value of ~1.4 mV/(cm.Oe) **[3]** in agreement with first-principles calculations **[4].** Actually, the linear ME effect in BFO is caused by the reorientation of the vector associated to the octahedral tilting under electric or magnetic field **[5]**. Therefore, any perturbation of the oxygen octahedral through the underlying Dzyaloshinsky-Moriya mechanism is a good strategy to perturb the cycloidal modulation and thus activate and enhance the ME response of BFO. For instance, epitaxial strains in thin films can be used to affect the oxygen octahedral rotation **[6]** through magnetoelastic effects **[7]**, which can even suppress the cycloidal spin order present in the bulk **[8]**, and in turn, increases the ME coefficients with values higher than the bulk ones **[9]**. Another approach for improving the ME properties of BFO keeping it in its bulk form is the doping. However, while doping or co-doping of bulk BFO on Bi- and/or Fe-site **[10-20]** is known to reduce the leakage current and enhances the magnetization, reports on ME measurements are rather rare **[11]** and most often indirect studies using e.g. magnetodielectric measurements are reported **[19-20]**. Here we use Co/Mn co-doping on $BiFeO_3$ bulk ceramic samples; Co is expected to increase the magnetic properties and Mn to reduce the leakage current and thus all in all to improve the magnetoelectric response which has never been reported yet considering such co-doping. In order to understand the role of each dopant on the magnetoelectric properties, we fix the amount of Co/Mn dopant to 10%, corresponding to the concentration one can typically insert into BFO, and we vary the ratio between Co and Mn by synthesizing $BiFe_{0.9}Co_xMn_{0.1-x}O_3$ with nominal concentration x=1, 3, 5, 7 and 9%.

2. Experimental

The chemical reagents used in this work are bismuth nitrate [$Bi(NO_3)_3.5H_2O$], iron nitrate [$Fe(NO_3)_3.9H_2O$],], hexa-ammine-cobalt chloride [$CoCl_3.6NH_3$], manganic acetylacetonate $Mn(C_5H_7O_2)_3$, nitric acid (HNO_3) and potassium hydroxide (KOH). All the chemicals are analytical grade purity and are used as received without further purification.

Stoichiometric proportions of $Bi(NO_3)_3$, $Fe(NO_3)_3$, $CoCl_3$, and $Mn(C_5H_7O_2)_3$ are dissolved in diluted HNO_3 and distilled water, respectively. After complete dissolution of the precursors, the three solutions are mixed. Then, KOH solution is slowly added to the above solution to coprecipitate Bi^{3+}, Fe^{3+}, Co^{3+} and Mn^{3+} ions under constant stirring and a brown colored precipitate forms. The precipitate is filtered and washed with distilled water to remove $(NO_3)^-$ and K^+ ions. Then, it is mixed with KOH solution under constant magnetic stirring for 30 min. The suspension solution is poured into a stainless-steel Teflon-lined autoclave for the hydrothermal treatment. The autoclave is sealed and maintained at 200 °C for 8h under continuous mechanical stirring. Finally, it is cooled down to room temperature naturally. The products is filtered, washed with distilled water several times, and then dried at 90 °C for 3 h and annealed at 750 °C for 2 h with a heating/cooling rate of 200 °C/h prior to characterizations **[21].**

The phases of the obtained samples are characterized by x-ray diffraction (XRD) (DRX, D8 ADVANCE, Bruker) in a $20° \leq 2\theta \leq 80°$ range of Bragg angle 2θ using Cu Kα ($\lambda_{1.2}$= 1.5406 Å) at room temperature. Differential thermal analyses (DTA) of the samples are performed in a Setaram Setsys Evolution TGA-DTA from room temperature to 900 °C under an argon atmosphere with a scanning rate of 10 °C / min to study the phase transition in the synthesized Co/Mn co-doped $BiFeO_3$. Differential scanning calorimetric (DSC) experiments are realized with a Q100 scanning calorimeter within a temperature range from 200 to 500 °C with a speed 10 °C / min of heating. Raman spectral measurements are performed at room temperature with a LABRAM Horiba Raman spectrometer in the range 100 cm^{-1} to 800 cm^{-1} using a 632.8 nm HeNe laser as excitation source. Room temperature dielectric measurements are performed using Agilent 4294A impedancemeter between 1 kHz and 1 MHz. Magnetic hysteresis loops are measured at room temperature by using a Physical Properties Measurement System (PPMS-6000) with a magnetic field. Magnetoelectric measurements are realized at room temperature on electrically pre-poled ceramics (8kV/cm applied in silicon oil from 200°C to room temperature) using an homemade set up based on lock-in technique where the generated voltage V_{ME} is recorded under a static magnetic field (H_{DC}) applied simultaneously in the transverse direction of the ceramic while a small alternating magnetic field (H_{AC}) using Helmoltz coils (10

Oe at 10 kHz) is superimposed in the same direction. The direct magnetoelectric coefficients α_{ME} are hence deduced from the piezoelectric voltage measured along the thickness t direction and given by $\alpha_{ME} = V_{ME} / (t.H_{AC})$.

3. Results and discussions

3.1 Structural characterization

Figure 1 shows X-ray diffraction (XRD) patterns of $BiFe_{0.9}Co_xMn_{0.1-x}O_3$ (BFCMO) with x=0.01, 0.03, 0.07, 0.09 and pure BFO ceramic samples sintered from the powder obtained by our mechanically-stirred hydrothermal method.

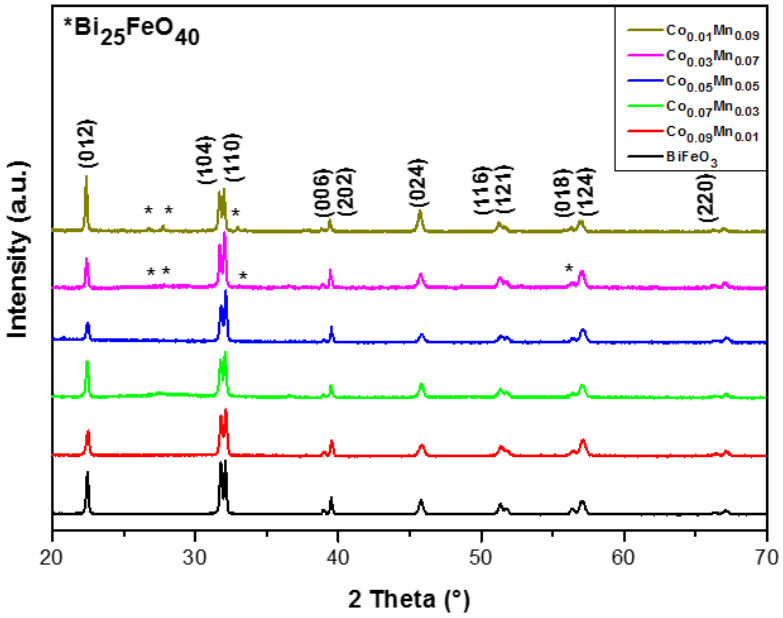

Fig.1 **.** XRD patterns of $BiFe_{0.9}Co_xMn_{0.1-x}O_3$ samples.

Bragg peaks indexation (in the hexagonal setting) indicates that all $BiFe_{0.9}Co_xMn_{0.1-x}O_3$ samples crystallize in the same symmetry as the pure BFO whatever the amount of co-doping, meaning into the space group R3c. No parasitic phase can be evidenced for $BiFe_{0.9}Co_xMn_{0.1-x}O_3$ samples up to x=0.05 and a secondary parasitic phase is seen (see stars in Fig. 1) for $x \leq 0.03$ and corresponds to the Sillenite phase $Bi_{25}FeO_{40}$. **Table 1** gathers the lattice parameters of the equivalent hexagonal unit cell extracted from the diffraction patterns as well as the corresponding volume for $BiFe_{0.9}Co_xMn_{0.1-x}O_3$ samples that we plotted in **Figure 2** as a function of the average radius of the co-dopant considering the ionic radii for Co^{3+} and Mn^{3+} being 61.0 pm and 65.0 pm respectively, in high spin state. Note that the Fe^{3+} radius is 64.5 pm, very close to that of Mn^{3+}. As expected the volume decreases going towards Co-rich concentration i.e. lowering the average radius **[11,22]**. This can be also seen **[11]** as a chemical pressure i.e. a

proxy hydrostatic pressure due to the different size of Co with respect to Mn (and Fe) depicted by the variation of the volume adding more Co at the place of Mn (Table 1). Changing from $BiFe_{0.9}Co_{0.01}Mn_{0.09}O_3$ to $BiFe_{0.9}Co_{0.09}Mn_{0.01}O_3$ corresponds to a volume variation of -0.97% i.e. ~1%. Taking the volume change under hydrostatic pressure which corresponds to 1 $Å^3$ per ~1.6 GPa **[23]** in case of pure BFO, it turns out that 1% of Co corresponds to ~0.21 GPa of chemical pressure **[11].** This chemical pressure and associated contraction strain should therefore affect the magnetoelectric properties as magnetoelastic effects are expected **[7].**

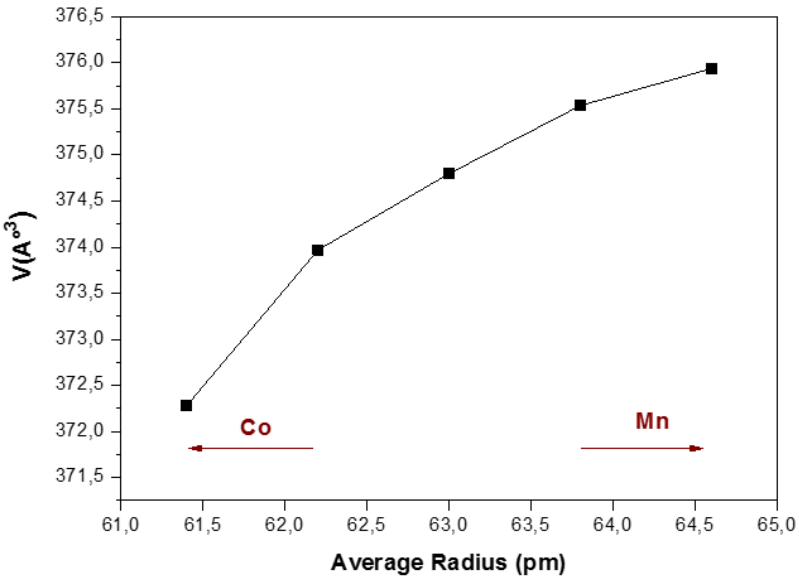

Fig.2. Volume evolution of $BiFe_{0.9}Co_xMn_{0.1-x}O_3$ as a function of the average radius of the co-dopant

Table.1. Room temperature crystal structure parameters, dielectric, magnetic and magnetoelectric properties of $BiFe_{0.9}Co_xMn_{0.1-x}O_3$ samples.

X Co	**0.01**	**0.03**	**0.05**	**0.07**	**0.09**
a (Å)	5.589(1)	5.587(1)	5.585(1)	5.581(1)	5.570(1)
Average radius	64.6	63.8	63	62.2	61.4
c (Å)	13.897(1)	13.892(1)	13.875(1)	13.864(1)	13.856(1)
V (Å³)	375.94(2)	375.54(1)	374.80(1)	373.97(2)	372.28(2)
$(V_x-V_{0.01Co})/V_{0.01Co}$	0	-0.11%	-0.30%	-0.52%	-0.97%
Mr (emu/g)	0.10(1)	0.76(1)	1.53(2)	2.42(3)	3.39(3)
Mm (emu/g)(~19kOe)	0.24(1)	0.98(2)	2.67(2)	3.58(3)	10.88(4)
ε_r (1MHz)	68	28	37	47	47
tan δ (1MHz)	0.77	0.11	0.04	0.11	0.42
T_N (°C)	381.4(3)	388.3(3)	395.7(3)	398.3(4)	404.7(5)

T_C (°C)	824.8(3)	827.7(4)	829.3(4)	830.5(4)	831.7(5)
α_{ME} (mv/(Oe.cm))	11.17(12)	5.14(9)	8.72(11)	7.85(7)	7.40(7)

To get further insights into the structure, we use Raman spectroscopy technique. **Figure 3** shows the Raman spectra at room temperature for all $BiFe_{0.9}Co_xMn_{0.1-x}O_3$ samples. According to group theory, 13 optical-phonon active modes ($4A_1$+9E) **[24]** are expected for R3c symmetry. One can see that all the spectra, except those coined as b) and d), are very similar showing 4 modes at 170, 221, 300 and 625 cm^{-1} which can be assigned to A_1-symmetry longitudinal optical modes [A_1-1, A_1-2,A_1-3, A_1-4 (LO)] and the 8 modes located at 73, 135, 258, 280, 346, 369, 438, 518 cm^{-1} which are associated with transverse optical E(TO) [E-1, E-2, E-3, E-5, E-6, E-7, E-8, E-9 (TO)] phonons. This shows that all our samples have the same symmetry as the one of pure BFO, in agreement with our XRD data. Moreover in case of $x \leq 0.03$ i.e. Mn-rich compositions, some of the Raman spectra (see Figure 3, spectra b) and d)) are different with regards to the one of BFO and are associated to the parasitic $Bi_{25}FeO_{40}$ phase we also evidenced using x-ray diffraction. Note that we also did several Raman measurements at different places for each sample (the diameter of the laser beam spot is about 2 µm) and the parasitic phase is only found for $x \leq 0.03$.

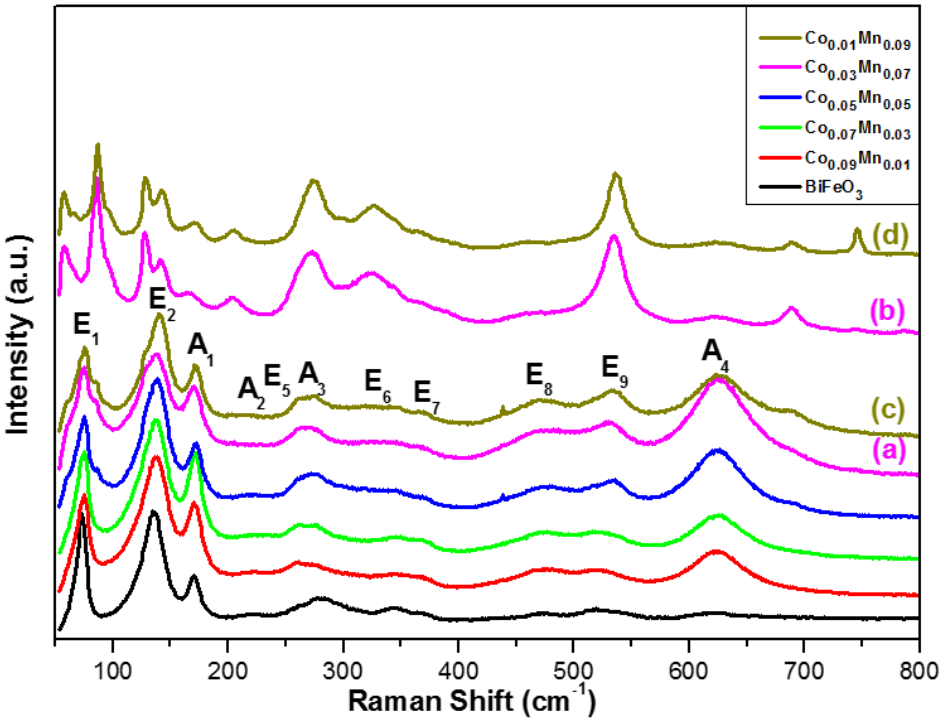

Fig.3. Raman scattering spectra of the BFCMO samples at room temperature.

The BFO Raman spectrum **[25]** is characterized by the contribution of the Bi atoms at the lower wavenumbers, i.e., up to 170 cm^{-1}, that of the Fe atoms mostly to the modes between 150 and

260 cm^{-1} and possibly to the modes present at higher frequencies, and the contribution of the oxygen motion which strongly governs the modes above 260 cm^{-1}.

When co-doped all the modes shift as shown on **Figure 4** and soften with increasing the amount of Co in the co-doping as e.g. illustrated with the E_2 mode position which decreases from 140.7 cm^{-1} to 137.5 cm^{-1}. This behavior can be linked to the volume decrease when Co amount increases we evidenced by x-ray diffraction. Another mode which is very sensitive to both Mn and Co substitution is the mode we coined as A_1-4 (**Figure 4**) whose intensity significantly increases (**Figure 3**) when BFO is doped with those elements. The activation of this wide band at 625 cm^{-1} is attributed to the distortion of the [$(Co,Mn,Fe)^{3+}O_6$] octahedra through Jahn-Teller effect due to the substitution of Fe^{3+} by Co^{3+} and Mn^{3+} as already observed in single Mn-doped $BiFeO_3$ and Co-doped $BiFeO_3$ compounds **[26,11].**

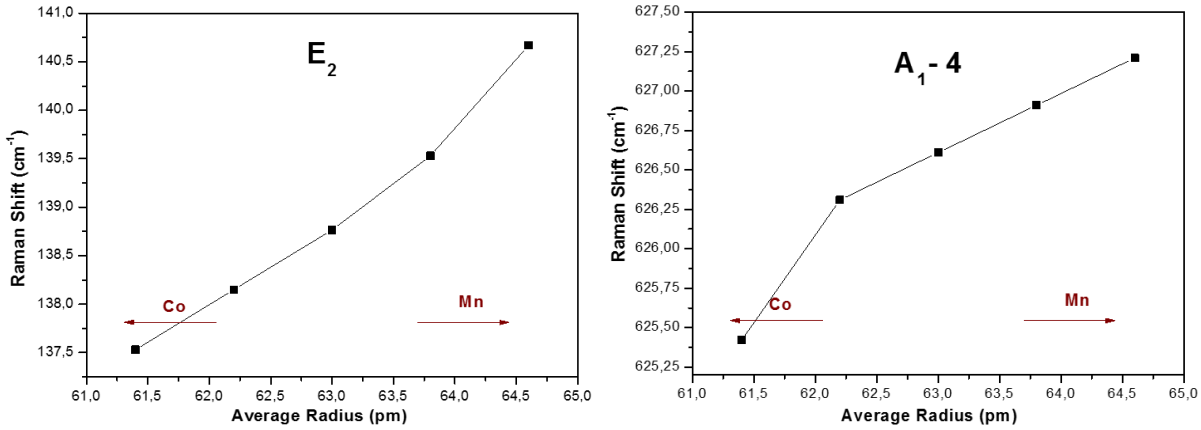

Fig.4. Raman modes E_2 and A_1-4 at room temperature as function of the average radius of the co-dopant.

3.2 Phase transitions

Thermal analysis using both DTA and DSC techniques are used to determine the temperatures of the ferroelectric and magnetic phase transitions. **Figure 5** (left) shows the DTA measurements carried out on $BiFe_{0.9}Co_xMn_{0.1-x}O_3$ samples displaying an endothermic peak between ~824 and ~832 °C that corresponds to the ferroelectric-to-paraelectric transition temperature (T_C). Adding more Co in the Co/Mn co-doping increases the critical temperature by about 7°C when changing from $BiFe_{0.9}Co_{0.01}Mn_{0.09}O_3$ to $BiFe_{0.9}Co_{0.09}Mn_{0.01}O_3$ as shown in **Figure 5** (right). As a consequence, because the polarization varies at first order like the square root of the temperature minus T_C, it should not vary, if any, at room temperature and thus the ambient electrical properties should remain unchanged compared to those of pure BFO. When having a closer look of the curves in Figure 5 (left) one can also notice an extra endothermic

peak at ~800 °C for Mn-rich compositions i.e. $x \leq 0.03$. This extra heat flux is likely to be related to the parasitic $Bi_{25}FeO_{40}$ phase **[27]**, in agreement with our x-ray diffraction and Raman spectroscopy data.

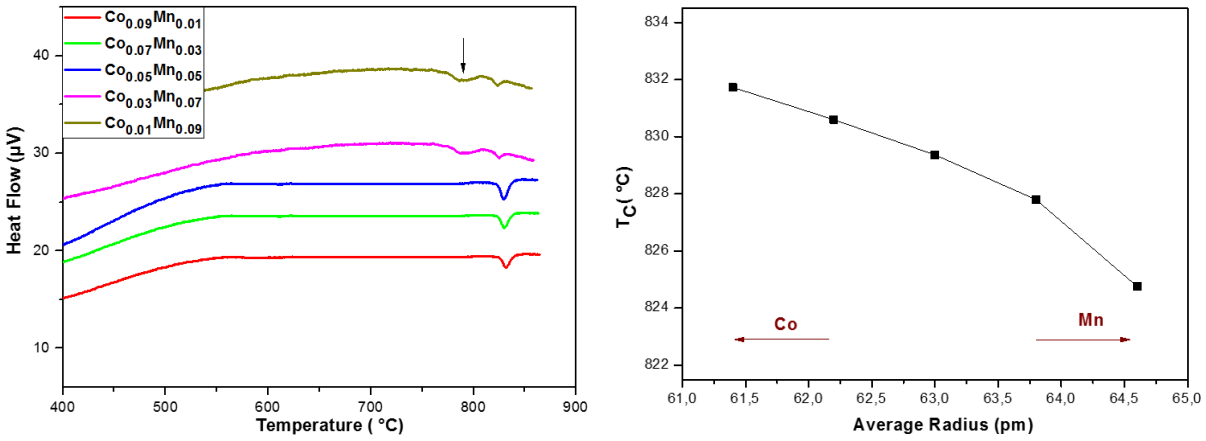

Fig.5. (left) DTA curves for $BiFe_{0.9}Co_xMn_{0.1-x}O_3$,
(right) Ferroelectric-to-Paraelectric T_C temperature extracted from the DTA curves as function of the average radius of the co-dopant.

Figure 6 (left) shows that the DSC heat flux exhibits an endothermic peak in each $BiFe_{0.9}Co_xMn_{0.1-x}O_3$ sample at about 380°C corresponding to the antiferromagnetic Néel temperature (T_N). As for T_C, T_N also increases by adding more Co in the Co/Mn co-doping but much strongly as T_N changes by up to 23°C when changing from $BiFe_{0.9}Co_{0.01}Mn_{0.09}O_3$ to $BiFe_{0.9}Co_{0.09}Mn_{0.01}O_3$ as shown in **Figure 6** (right). This is in agreement with previous observation in Co doped-BFO **[11]** and can be understood by the fact that Co/Mn co-doping affects directly the Fe-site which carries the magnetic proprieties. Indeed according to mean field theory, the transition Néel temperature T_N is approximated as $JS(S+1)/ k_B$ where J is the exchange coupling, S the total spin and k_B the Boltzmann's coefficient. J the exchange interaction is directly related to the Fe-O-Fe angle and Fe-Fe distance and thus changing Fe by Co/Mn should impact J. As seen previously, especially Co ions induces a chemical pressure that reduces the volume of the unit cell. As a result, the distance between magnetic moments carried by the Fe/Co/Mn is reduced. Consequently as J is known to scale inversely proportional to the this distance **[28]**, it increases which results in T_N increasing for Co-rich compositions as observed in **Figure 6** (right).

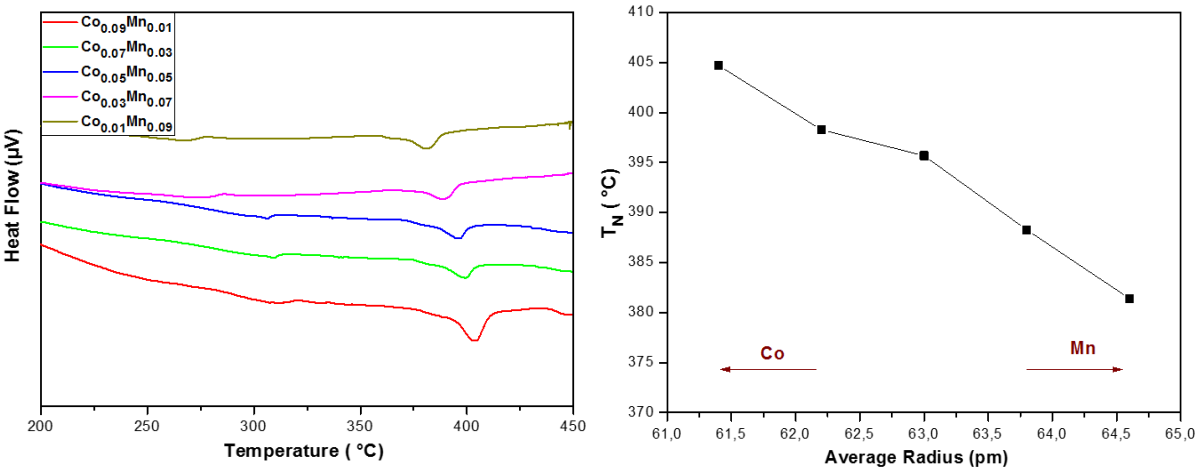

Fig.6. (left) DSC curves for $BiFe_{0.9}Co_xMn_{0.1-x}O_3$, (right) Antiferromagnetic-to-Paramagnetic T_N temperature extracted from the DSC curves as function of the average radius of the co-dopant. Note that the extra heat peak observed in the range 280°C-310°C has been ascribed to skin effect **[29]**.

3.3 Dielectric and magnetic characterization

Figure 7 (left) displays the dielectric constant (ε_r) value (and tan δ dielectric losses in inset) at room temperature at different frequencies for each of our samples. With changing the amount of Co/Mn, the dielectric constant and losses vary only weakly with the composition and frequency measurement, except for the Mn-richer composition $BiFe_{0.9}Co_{0.01}Mn_{0.09}O_3$. The strong dielectric variation for $BiFe_{0.9}Co_{0.01}Mn_{0.09}O_3$ with frequency is likely due to the presence of the parasitic phase which leads to high losses reaching tan δ ~70%. For the other compositions (see Table), the dielectric constant at 1 MHz varies between 30 and 50 with losses ranging between 3% and 40%. Those values are very comparable to those of pure BFO reported in the literature **[30]** and thus confirm our expectations concerning the unchanged polar properties with our co-doping from the variation of T_C we observed. However, as the Néel temperature T_N has significantly changed and in link with the Jahn-Teller-active Raman mode we observed, the magnetic response should change. **Figure 7** (right) shows the magnetic hysteresis loops (M-H) of $BiFe_{0.9}Co_xMn_{0.1-x}O_3$ samples at room temperature measured using PPMS with an applied magnetic field of 20000 Oe.

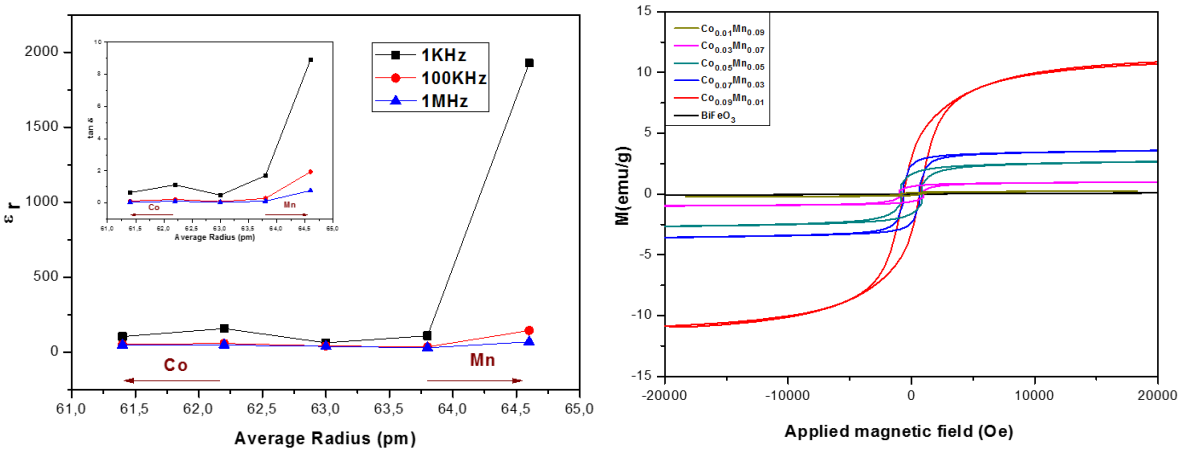

Fig.7. (left) Room temperature dielectric constant (ε_r) (and dielectric tan δ losses) at 1 kHz, 100 kHz and 1 MHz as function of the average radius of the co-dopant, (right) M-H curves of $BiFe_{0.9}Co_xMn_{0.1-x}O_3$ at room temperature**.**

While pure BFO is antiferromagnetic with a very weak canting-based ferromagnetic moment, the ferromagnetic hysteresis loop grows up by increasing Co content in the co-dopant as shown in **Figure 7** (right) and **Table**. For the Co-richer composition i.e. $BiFe_{0.9}Co_{0.09}Mn_{0.01}O_3$, the remanent Mr and Mm maximum magnetization are significantly increased reaching Mr = 3.394 emu/g and Mm =10.884 emu/g at 19KOe. Such increase cannot be accounted to parasitic phases as our structural data do not reveal them for this latter composition. Note that the Mn-rich compositions for which we evidenced the parasitic $Bi_{25}FeO_{40}$ phase give the worst magnetic response i.e. weaker ferromagnetic loop and $Bi_{25}FeO_{40}$ phase is paramagnetic at room temperature **[27]**, so the parasitic phase cannot explain the enhancement of the magnetization for Co-rich Co/Mn co-doped BFO system and rather we suggest that partial substitution of Fe^{3+} (d^5 electronic configuration) by Co^{3+} (d^6) favors double exchange interactions as we showed that Co substitution reduces the unit cell volume and thus favors exchange interactions through the diminution of Fe-O-Fe angle and Fe-Fe distance.

3.4 Magnetoelectric characterization

As already stressed, direct measurements of magnetoelectric (ME) coupling are rather scarce. Here, we measure ME coefficient at room temperature of the Co/Mn co-doped BFO ceramics as a function of an applied magnetic field (H) at a frequency of 10 kHz as displayed in **Figure 8** (left). The values of magnetoelectric coefficients are listed in Table 1 and plotted in **Figure 8** (right) as a function of the average radius of the co-dopant of $BiFe_{0.9}Co_xMn_{0.1-x}O_3$ samples.

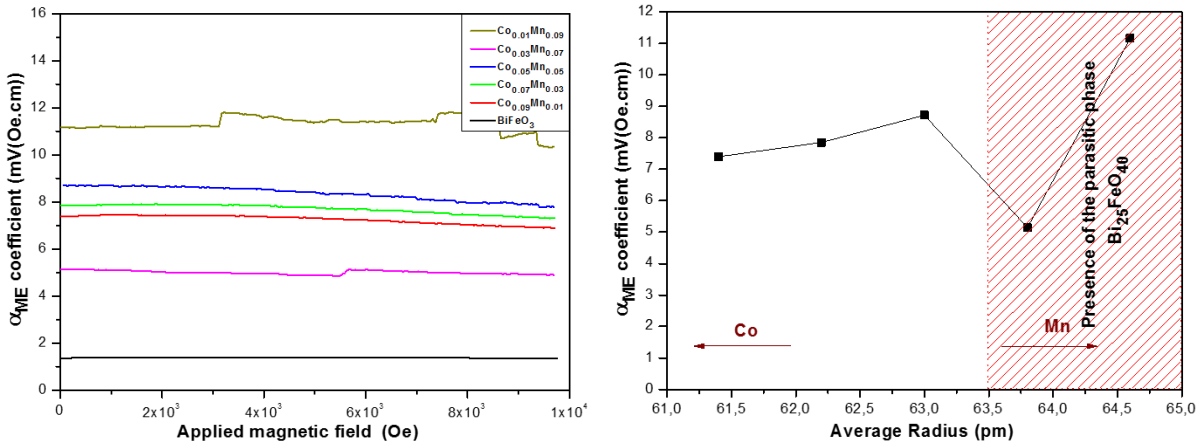

Fig.8 (left) Magnetoelectric (ME) coefficient dependence on applied magnetic field of $BiFe_{0.9}Co_xMn_{0.1-x}O_3$ samples. The jumps on samples x=0.01 and x=0.03 could be due to the presence of the parasitic phases (right) ME coefficient evolution as function of the average radius of the co-dopant.

All the $BiFe_{0.9}Co_xMn_{0.1-x}O_3$ samples show a linear ME effect in the presence of the DC applied magnetic field. A significant improvement in the ME coefficient by up to 6 times is obtained when compared to pure BFO (1.4 mV/(Oe.cm)). Note that the value we obtain for BFO is similar to the reported one **[3]**. The substitution of Fe by Co/Mn is believed to destabilize the cycloidal spin modulation which is at the origin of the weak ME coupling in BFO **[11]**. Note that the Jahn-Teller effect we evidenced using Raman spectroscopy may also contribute by destroying the long period (64 nm) spin modulation of BFO. For the Co-richer composition i.e. $BiFe_{0.9}Co_{0.09}Mn_{0.01}O_3$ as the ME coefficient is 7.400 mV/(Oe.cm) and increases by ~18% for composition $BiFe_{0.9}Co_{0.05}Mn_{0.05}O_3$ (8.720 mV/(Oe.cm)). For the Mn-richer compositions, unfortunately while the ME coefficient reaches 11,166 mv/(Oe.cm) for $BiFe_{0.9}Co_{0.01}Mn_{0.09}O_3$ this value cannot be considered as purely intrinsic as we evidenced parasitic phases as well as important electrical losses.

4. Conclusion

In this work we show the effect of Co and Mn co-doping on structural, magnetic, dielectric and magnetoelectric properties in BFO synthesized using a stirred hydrothermal route. By increasing the amount of Co in the co-doped samples, we demonstrate an increase on the antiferromagnetic (T_N) transition temperature (up to 23°C) with an improvement of the magnetic properties compared to that of pure BFO i.e. Mr ($BiFe_{0.9}Co_{0.09}Mn_{0.01}O_3$)=3.394 emu/g against Mr ($BiFeO_3$)=0.002 emu/g. Furthermore, we show that by 50-50 % of Co and Mn co-doping $BiFe_{0.9}Co_xMn_{1-x}O_3$ we can significantly enhance the magnetoelectric coupling

with a ME coefficient= 8.720 mV/(Oe.cm) i.e. up to 6 times higher than that of pure $BiFeO_3$. Moreover, we note that the presence of parasitic phases in Mn-rich samples impacts the magnetoelectric coupling and the dielectric properties in which we find unwanted strong dielectric losses.

References

[1] N.A. Spaldin, R. Ramesh, Nature Mater., 2019, **18**, 203–212
[2] G. Catalan, J.F. Scott, Adv. Mater., 2009, **21**, 2463-2485
[3] S.V. Vijayasundaram, G. Suresh, R.A. Mondal, R. Kanagadurai, J. Magn. Magn. Mater., 2016, **418**, 30-36
[4] I.A. Kornev, S. Lisenkov, R. Haumont, B. Dkhil, L. Bellaiche , Phys. Rev. Lett., 2007, **99**, 227602
[5] A.F. Popkov, M.D. Davydova, K.A. Zvezdin, S.V. Solovyov, A.K. Zvezdin, Phys. Rev. B, 2016, **93**, 094435
[6] I.C. Infante, J. Juraszek, S. Fusil, B. Dupé, P. Gemeiner, O. Diéguez, F. Pailloux, S. Jouen, E. Jacquet, G. Geneste, J. Pacaud, J. Íñiguez, L. Bellaiche, A. Barthélémy, B. Dkhil, M. Bibes, Phys. Rev. Lett., 2011, **107**, 237601
[7] A. Agbelele, D. Sando, C. Toulouse, C. Paillard, R.D. Johnson, R. Rüffer, A.F. Popkov, C. Carrétéro, P. Rovillain, J.M. LeBreton, B. Dkhil, M. Cazayous, Y. Gallais, M.A. Méasson, A. Sacuto, P. Manuel, A.K. Zvezdin, A. Barthélémy, J. Juraszek, M. Bibes, Adv. Mater., 2017, **12**, 1602327-1602335
[8] D. Sando, A. Agbelele, D. Rahmedov, J. Liu, P. Rovillain, C. Toulouse, I.C. Infante, A.P. Pyatakov, S. Fusil, E. Jacquet, C. Carrétéro, C. Deranlot, S. Lisenkov, D. Wang, J-M. Le Breton, M. Cazayous, A. Sacuto, J. Juraszek, A.K. Zvezdin, L. Bellaiche, B. Dkhil, A. Barthélémy, M. Bibes, Nature Mater., 2013, **12**, 641-646
[9] J. Wang J, J.B. Neaton, H. Zheng, V. Nagarajan, S.B. Ogale, B. Liu, D. Viehland, V. Vaithyanathan, D.G. Schlom, U.V. Waghmare, N.A. Spaldin, K.M. Rabe, M. Wuttig, R. Ramesh, Science, 2003, **299**, 1719-22
[10] V.A. Khomchenko, D.A. Kiselev, I.K. Bdikin, V.V. Shvartsman, P. Borisov, W. Kleemann, J.M. Vieira, A.L. Kholkin, Appl. Phys. Lett., 2008, **93,** 262905-1262905
[11] A. Marzouki, H. Harzali, V. Loyau, P. Gemeiner, K. Zehani, B. Dkhil, L. Bessais, A. Megriche, Acta Materialia. 2018, **145,** 316-321
[12] Q. Zhang, C.H. Kim, Y.H. Jang, H.J. Hwang, J.H. Cho, Appl. Phys. Lett., 2010, **96,** 152901
[13] K.G. Yang, Y.L. Zhang, S.H. Yang, B. Wang, J. Appl. Phys., 2010, **107,** 124109-1.199
[14] V.R. Singh, V.K. Verma, K. Ishigami, G. Shibata, Y. Yamazaki, A. Fujimori, Y. Takeda, T. Okane, Y. Saitoh, H. Yamagami, Y. Nakamura, M. Azuma, Y. Shimakawa, J. Appl. Phys., 2013, **114,** 103905-1103905
[15] T. Kawae, Y. Teraguchi, M. Kumeda, A.Morimoto, Appl. Phys. Lett., 2009, **94,** 112904-1112904
[16] W. Sakamoto, A. Iwata, M. Moriya, T. Yogo, Mater. Chem. Phys., 2009, **116**, 536
[17] D. Varshney, G. Das, A. Kumar, AIP Conf. Proc., 2011, **1349,** 251
[18] K. Chakrabarti, B. Sarkar, S. Ghosh, S.K. De, G. Sinha, J. Lahtinen, Appl. Phys. Lett., 2012, **101**, 042401-1042401
[19] V.A. Reddy, N.P. Pathak, R. Nath, Solid State Comm., 2013, **171**, 40–45
[20] M.J. Miah, M.N.I. Khan, A.K.M. Hossain, J. Magn. Magn. Mater., 2016, **379**, 39-50

[21] A. Marzouki, H. Harzali, F. Saida, A. Megriche, K. Zehani, L. Bessais, J. Tunisian Chem. Soc., 2016, **18,** 38-42
[22] K.S. Kumar, P. Aswini, C. Venkateswaran, J.Magn. Magn. Mater., 2014, **364**, 60–67
[23] M. Guennou, P. Bouvier, G.S. Chen, B. Dkhil, R. Haumont, G. Garbarino, J. Kreisel, Phys. Rev. B, 2011, **84,** 174107
[24] Y. Zheng, G. Tan, A. Xia, H. Ren, J. Alloys Compd., 2016, **684**, 438-444
[25] A.A. Porporati, K. Tsuji, M. Valant, A.K. Axelsson, G. Pezzotti, J. Raman Spectrosc., 2010, **41**, 84-87
[26] L. Chen, L. Zheng, Y. He, J. Zhang, Z. Mao, X. Chen, J. Alloys Compd., 2015, **633**, 216–219
[27] R. Koferstein, T. Buttlar, S.G. Ebbinghaus, J. Solid State Chem., 2014, **217**, 50-56
[28] L.E. Gontchar, A.E. Nikiforov, Phys. Rev. B, 2002, **66**, 014437
[29] X. Marti et al., Phys Rev. Lett., 2011, **106**, 236101
[30] S. Skiadopoulou, V. Goian, C. Kadlec, F. Kadlec, X.F. Bai, I.C. Infante, B. Dkhil, C. Adamo, D.G. Schlom, S. Kamba, Phys. Rev. B, 2015, **91**, 174108